Spin-dependent Hall effect in semiconductors

J.-N. Chazalviel
Laboratoire de Physique de la Matière Condensée, Ecole Polytechnique, Paris, France*
(Received 25 November 1974)

We recall the theory of the spin-dependent Hall effect in semiconductors and give an elementary presentation, stressing the physical aspects of the problem. The spin-dependent Hall effect arises from the spin-orbit interaction in the crystal, via the admixture of p states into the conduction-band Bloch functions. A remarkable consequence of this admixture is the existence of the so-called *periodic part of* $\vec{r}$, which can be interpreted as a transverse displacement of the spin-polarized electron. This transverse displacement yields a first contribution to the spin-dependent Hall effect; the *displacement contribution* corresponds to a side jump of the electron upon scattering and gives a transverse conductivity independent of the scattering process. A second contribution to the spin-dependent Hall effect is the *skew scattering*, due to a left-right asymmetry of the scattering cross section. Next, we report the experimental study of the spin-dependent Hall effect in n-type indium antimonide. The spin-dependent Hall effect is unambiguously separated from the much larger ordinary Hall effect by using a spin-resonance method. The study of the effect on a series of samples of various doping levels evidences the presence of the two contributions. In the weakly doped samples, only the displacement contribution remains, and the measurements agree, without any adjustable parameter, with the theoretical predictions for the transverse mobility $\mu_{yx}^{D} = -160$ cm^2/V sec. For higher concentrations, the skew scattering becomes notable, cancelling the displacement contribution and changing the sign of the over-all effect. The contribution of multiple scattering to this process appears to be dominant; a semiempirical calculation is given, which agrees with experiment within a factor of 2. Finally, we report the study of the spin-dependent Hall effect in highly doped n-type germanium. The necessary extensions of the theory are presented. The study of the effect as a function of temperature in a sample with $N_D \approx 3.1 \times 10^{17}$ cm^{-3} reveals a behavior quite similar to that observed in the case of InSb. At low temperature, the displacement contribution is observed alone and is found to be in good agreement with theory ($\mu_{yx}^{D} = -0.20$ cm^2/V sec) without any adjustable parameter. At higher temperature, the skew scattering increases and changes the sign of the observed effect. A model with two kinds of carriers is shown to account for the observed temperature dependence.

I. INTRODUCTION

In the last 20 years, the giant transverse conductivity observed for a long time in ferromagnetics has become the source of an abundant literature and of many controversies between theorists.[1-8] Two kinds of theories were proposed to explain this *extraordinary Hall effect* in magnetized materials: The theories of the first kind start from the band-magnetism model (one electronic system); the others consider an Heisenberg magnet with nonmagnetic conduction electrons (two electronic systems). In both cases the extraordinary Hall effect must arise from some spin-orbit interaction, either direct in the first model, or spin–other-orbit interaction in the case of two electronic systems. Moreover, the diversity of the possible scattering processes led to a great number of papers, but none of them yielded good agreement with experiment, the theoretical results being often several orders of magnitude too small. This failure is probably ascribable to the extreme complexity of ferromagnetic systems at finite temperature and to the lack of knowledge on the band structure of these materials.

The leading idea of our work is that a transverse conductivity should also exist in a magnetized semiconductor and the theory in this case should be much simpler since the electron wave functions in these materials are well known and their band structures have been extensively studied. The experimental difficulty, however, is that there is no spontaneous magnetization and the spin-dependent Hall effect must be separated from the much larger ordinary Hall effect. In a preliminary experiment, we have shown this to be possible by using a spin-resonance method.[9]

At the same time, some theorists have worked out the theory of the spin-dependent Hall effect in direct-gap III-V semiconductors.[10-12] It falls under the category of the theories with a single electronic system and mostly confirms the validity of the pioneering work of Luttinger.[4] The purpose of the present contribution is to report an experimental study of the spin-dependent Hall effect in some of those simple nonmagnetic systems, thus providing an unambiguous check of the theory.

In Sec. II, we recall the theoretical background relevant to semiconductors. The theoretical results, usually obtained from lengthy calculations,

are shown to bear on a very simple physical concept. In Sec. III, we present the experimental study of the spin-dependent Hall effect in n-type indium antimonide, which is a direct application of the theory given in Sec. II. In Sec. IV, we consider the spin-dependent Hall effect in n-type germanium. This case is most favorable experimentally, but it requires some extensions of the theory because of the peculiar aspects of the band structure of this semiconductor.

II. THEORY FOR A DIRECT-GAP III-V SEMICONDUCTOR

We first recall the band structure of a III-V semiconductor and give the expressions of the wave functions of the conduction band. Then we consider the matrix elements of the position operator $\vec{r}$, which permits us to introduce the physical concept of the *transverse displacement* of a wave packet. This concept will be shown to be the clue to the intuitive comprehension of the spin-dependent Hall effect.

A. Band structure and wave functions for a III-V semiconductor

The band structure of a III-V semiconductor exhibits a direct gap, located at the center of the first Brillouin zone ($\vec{k}=0$).[13] The eigenfunctions of the crystal Hamiltonian can be chosen of the Bloch type:

$$\Psi_{n\vec{k}\sigma} = u_{n\vec{k}\sigma}\, e^{i\vec{k}\cdot\vec{r}} , \tag{1}$$

where n and σ are, respectively, the band and spin index, and $u_{n\vec{k}\sigma}$ has the lattice periodicity. At the point $\vec{k}=0$, the conduction-band Bloch functions are s-like ($u_{0\sigma}=|s\sigma\rangle$) and the valence-band states ($|X\sigma\rangle$, $|Y\sigma\rangle$, $|Z\sigma\rangle$) are p-like. The valence-band degeneracy is partially lifted by spin-orbit interaction. Hereafter we call E_g the band gap and Δ the spin-orbit splitting of the valence band. The expressions of $u_{n\vec{k}\sigma}$ near the $\vec{k}$ origin may be derived by $\vec{k}\cdot\vec{p}$ perturbation theory from the $\vec{k}=0$ wave functions and energy levels.[14] If one takes into account only the lower conduction band and the three upper valence bands, the calculation may even be carried out exactly. The neglect of other bands is generally a good approximation, especially in InSb, where the band gap is much smaller than the other interband spacings. The resulting $u_{n\vec{k}\sigma}$ have been given by Zawadzki[15]; since in our case the Fermi energy E_F is much smaller than E_g, we keep only the terms up to second order in $\vec{k}$; the periodic parts of the Bloch functions for the conduction band then become

$$u_{\vec{k}\sigma} = a|s\sigma\rangle - \frac{i\hbar P}{3m}\left[\left(\frac{2}{E_g}+\frac{1}{E_g+\Delta}\right)\vec{k}\cdot|\vec{R}\sigma\rangle + i\left(\frac{1}{E_g}-\frac{1}{E_g+\Delta}\right)2\vec{S}\cdot(\vec{k}\times|\vec{R}\sigma\rangle)\right], \tag{2}$$

with

$$a = 1-\frac{1}{2}\,\frac{E}{E_g}\,\frac{3E_g^2+4E_g\Delta+2\Delta^2}{(3E_g+2\Delta)(E_g+\Delta)} \quad ;$$

here $\vec{S}$ is the spin operator and $|\vec{R}\sigma\rangle$ is the vector of components $|X\sigma\rangle$, $|Y\sigma\rangle$, $|Z\sigma\rangle$. The matrix element $\langle s|p_x|X\rangle$ has been noted iP. The band index in $u_{\vec{k}\sigma}$ has been omitted, since we are concerned only with the conduction-band wave functions.

B. Matrix elements of $\vec{r}$: Transverse displacement

It has been known for a long time that the matrix elements of $\vec{r}$ between Bloch states can be formally separated into two parts, by performing an integration by parts[2,16-18]

$$\langle\vec{k}\sigma|\vec{r}|\vec{k}'\sigma'\rangle = \frac{1}{i}\,\vec{\nabla}_{\vec{k}'}\,\delta(\vec{k}-\vec{k}') - \frac{1}{i}\,\delta(\vec{k}-\vec{k}')\iiint_{\Omega} u^*_{\vec{k}\sigma}\,\vec{\nabla}_{\vec{k}'}\,u_{\vec{k}'\sigma}\,\frac{d^3r}{\Omega} , \tag{3}$$

where Ω is the volume of a unit cell. In the case of plane-wave states (free electrons), the second member of Eq. (3) would reduce to its first term ("plane-wave part" of $\vec{r}$). The second term, hereafter noted as $\vec{R}$, arises from the periodic part of the Bloch function $u_{\vec{k}\sigma}$ and is usually called "periodic part" of $\vec{r}$.

Some authors have proposed that $\vec{R}$ corresponds to a "polarization" of the wave function inside a unit cell.[19,20] This picture is to our sense unsatisfactory. In fact, the physical meaning of $\vec{R}$ may be evidenced by considering a wave packet rather than plane-wave states. Although theoretically equivalent, the former point of view provides better insight to the problem.

We therefore define a wave packet by the development of its wave function along the basis Bloch states

$$\Psi = \iiint \frac{d^3k}{(2\pi)^3}\, u_{\vec{k}\sigma}(\vec{r})\, e^{i\vec{k}\cdot\vec{r}} f(\vec{k}) . \tag{4}$$

We suppose the function $f(\vec{k})$ to be localized in the Brillouin zone around some mean wave vector $\vec{\bar{k}}$. We can thus write

$$u_{\vec{k}\sigma}(\vec{r}) \approx u_{\vec{\bar{k}}\sigma}(\vec{r}) + (\vec{k}-\vec{\bar{k}})\,[\vec{\nabla}_{\vec{k}}\,u_{\vec{k}\sigma}(\vec{r})]_{\vec{k}=\vec{\bar{k}}} . \tag{5}$$

By inserting Eq. (5) into Eq. (4), the expression of Ψ becomes

$$\Psi = \{G(\vec{r})\, u_{\vec{k}\sigma}(\vec{r}) + (1/i)[\vec{\nabla}_{\vec{k}}\, u_{\vec{k}\sigma}(\vec{r})]_{\vec{k}=\vec{\bar{k}}} \cdot [\vec{\nabla}_{\vec{r}}\, G(\vec{r})]\}\, e^{i\vec{\bar{k}}\cdot\vec{r}} , \tag{6}$$

where

$$G(\vec{r}) = \iiint \frac{d^3k}{(2\pi)^3} f(\vec{k})\, e^{i(\vec{k}-\vec{\bar{k}})\cdot\vec{r}}$$

is the wave-packet envelope function. In the case of free electrons $[u_{\vec{k}\sigma}(\vec{r}) \equiv 1]$, the expression of Ψ would reduce to $G(\vec{r})\, e^{i\vec{\bar{k}}\cdot\vec{r}}$. The influence of $u_{\vec{k}\sigma}$ is double: First, Ψ is multiplied by $u_{\vec{k}\sigma}(\vec{r})$, a trivial result; to this level there is a "polarization" of the wave function inside a unit cell; however, the envelope function is unchanged and the average value of $\vec{r}$ for the wave packet is not affected. Second, an additional term appears in Ψ; this term is proportional to $\vec{\nabla}_{\vec{r}} G(\vec{r})$, and thus results in a *displacement of the envelope function*. Taking this term into account, the average position of the wave packet is modified by the quantity

$$\vec{R} = i \iiint_{\Omega} u^*_{\vec{k}\sigma}\, \vec{\nabla}_{\vec{k}}\, u_{\vec{k}\sigma}\, \frac{d^3r}{\Omega} . \tag{7}$$

This corresponds exactly to the previously mentioned periodic part of $\vec{r}$, which then appears as a displacement of the center of mass of the wave packet, and can be greater than a lattice constant.[21] (See Fig. 1.)

In the case of a III-V semiconductor, the value of $\vec{R}$ can be obtained by carrying in Eq. (7) the expression of the periodic part of the Bloch function $u_{\vec{k}\sigma}$ [Eq. (2)]. The result is

$$\vec{R} = \lambda \vec{S} \times \vec{k} \quad \text{or} \quad \vec{\nabla}_{\vec{k}} \times \vec{R} = 2\lambda \vec{S} , \tag{8}$$

with

$$\lambda = \frac{2\hbar^2 P^2}{3m^2}\left(\frac{1}{E_g^2} - \frac{1}{(E_g+\Delta)^2}\right) = \left(1 - \frac{g^*}{2}\right)\frac{\hbar^2}{m}\,\frac{2E_g+\Delta}{E_g(E_g+\Delta)} . \tag{9}$$

This displacement is transverse (i.e., perpendicular to the wave vector $\vec{k}$), proportional to the spin $\vec{S}$ and to the spin-orbit interaction; this is stressed in Eq. (9) by the presence of the factor $(2 - g^*)$ in the expression of λ.

C. Spin-dependent Hall effect: Displacement contribution ($\omega\tau \gg 1$)

The transverse displacement of a spin-polarized electron provides a straightforward contribution to the extraordinary Hall effect. Let us consider a polarized electron ($\vec{S} \parallel \vec{z}$) in an electric field $\vec{E}$ ($\vec{E} \parallel \vec{x}$) and neglect the collisions. This would correspond to the hypothetical case of an ac electric field, of frequency $\omega/2\pi$ much larger than the momentum relaxation rate $1/\tau$ ($\omega\tau \gg 1$).

The motion of the wave packet is described by the time dependence of $f(\vec{k})$, which is given by

$$i\hbar \frac{\partial f(\vec{k})}{\partial t} = \frac{\hbar^2 \vec{k}^2}{2m^*} f(\vec{k}) + \sum_{\vec{k}'} e\vec{E} \langle \vec{k}\sigma | \vec{r} | \vec{k}'\sigma \rangle f(\vec{k}') .$$

Here $-e$ is the electron charge ($e > 0$). From the expression of the matrix elements of $\vec{r}$ in the basis Bloch states, this can be written

$$i\hbar \frac{\partial f(\vec{k})}{\partial t} = \frac{\hbar^2 \vec{k}^2}{2m^*} f(\vec{k}) + eE_x \left(X + i\frac{\partial}{\partial k_x}\right) f(\vec{k}) . \tag{10}$$

The transverse velocity of the wave packet can be expressed as a function of $f(\vec{k})$ and $\partial f(\vec{k})/\partial t$,

$$\frac{dy}{dt} = \frac{d}{dt} \iiint f^*(\vec{k}) \left(Y + i\frac{\partial}{\partial k_y}\right) f(\vec{k})\, \frac{d^3k}{(2\pi)^3}$$

$$= \iiint \left[\frac{\partial f^*(\vec{k})}{\partial t}\left(Y + i\frac{\partial}{\partial k_y}\right) f(\vec{k}) + f^*(\vec{k})\left(Y + i\frac{\partial}{\partial k_y}\right)\frac{\partial f(\vec{k})}{\partial t}\right] \frac{d^3k}{(2\pi)^3} .$$

By carrying the expression of $\partial f(\vec{k})/\partial t$ [Eq. (10)] into Eq. (11) it gives

$$\frac{dy}{dt} = \frac{-eE_x}{\hbar} \iiint f^*(\vec{k}) \left(\frac{\partial Y}{\partial k_x} - \frac{\partial X}{\partial k_y}\right) f(\vec{k})\, \frac{d^3k}{(2\pi)^3} . \tag{11}$$

If $f(\vec{k})$ is localized on the scale of the first Brillouin zone, this reduces to

$$\frac{dy}{dt} \approx -\frac{eE_x}{\hbar}\left(\frac{\partial Y}{\partial k_x} - \frac{\partial X}{\partial k_y}\right) . \tag{12}$$

Therefore the application of an external electric field results in a non-null transverse velocity of the electron. This yields a transverse conduc-

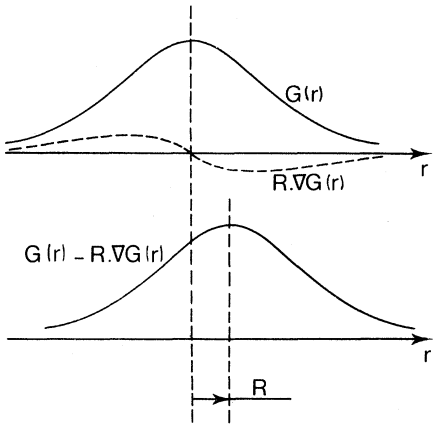

FIG. 1. Displacement of a Bloch electron. For free-electron states the wave-packet envelope function would be $G(\vec{r})$, the Fourier transform of $f(\vec{k} + \vec{\bar{k}})$. The existence of the periodic parts of the Bloch functions yields a further contribution $-\vec{R}\cdot\vec{\nabla}G(\vec{r})$, which is seen to produce a shift $\vec{R}$ of the wave-packet envelope function.

tivity

$$\sigma_{yx} = -\frac{ne}{E_x}\frac{dy}{dt} = \frac{ne^2}{\hbar}\left(\frac{\partial Y}{\partial k_x} - \frac{\partial X}{\partial k_y}\right) . \qquad (13)$$

The first term in Eq. (13) can be identified as the time variation of Y when the electron is accelerated by the electric field: Starting from the classical equation $\hbar dk_x/dt = -eE_x$, a naive reasoning would give $dy/dt = dY/dt = (-eE_x/\hbar)\,\partial Y/\partial k_x$; hence $\sigma^a_{yx} = (ne^2/\hbar)\,\partial Y/\partial k_x$. In fact, the occurrence of X in the matrix elements of the perturbation $e\vec{E}\cdot\vec{r}$ provides an extra contribution $\sigma^b_{yx} = -(ne^2/\hbar)\,\partial X/\partial k_y$, leading to the final Eq. (13). This result is physically satisfactory, since it depends only on $\vec{\nabla}_{\vec{k}}\times\vec{R}$, and is thus phase invariant (see footnote 21).

In a III-V semiconductor, using Eq. (8), Eq. (13) reduces to

$$\sigma_{yx} = \frac{ne^2}{\hbar}\lambda\langle 2S_z\rangle .$$

If one defines a transverse mobility by $\sigma_{yx} = ne\mu_{yx}$, then

$$\mu_{yx} = \frac{e\lambda}{\hbar} = \left(1 - \frac{g^*}{2}\right)\frac{\hbar e}{mE_g}\,\frac{2E_g + \Delta}{E_g + \Delta}\langle 2S_z\rangle . \qquad (14)$$

A typical order of magnitude is obtained with the band parameters of InSb; in this case $\mu_{yx} = 160$ cm^2/V sec for a spin-up electron.

D. Displacement effect: Role of the collisions ($\omega\tau \ll 1$)

For a dc electric field, the problem is far more difficult and has been the subject of many theories.[3-8,11] The simplest formulation has been given by Nozières and Lewiner.[12] Here we summarize their results and show that our concept of displacement of the wave packet provides a simple interpretation for the various terms, whose physical significance was, until recently, obscured by the high degree of complexity of the calculations.

The transverse conductivity, as given by Nozières and Lewiner, is the sum of six terms[22]:

$$\sigma^D_{yx} = \sigma^a_{yx} + \sigma^b_{yx} - \sigma'^a_{yx} - \sigma'^b_{yx} - \sigma''^a_{yx} - \sigma''^b_{yx} . \qquad (15)$$

In the limiting case $\omega\tau \ll 1$, one has $\sigma^a_{yx} = \sigma'^a_{yx} = \sigma''^a_{yx}$ and $\sigma^b_{yx} = \sigma'^b_{yx} = \sigma''^b_{yx}$; thus four among the six terms cancel each other, leading to a transverse conductivity opposite to the collisionless result [Eq. (13)]. The first two terms in Eq. (15) are those previously encountered in the case $\omega\tau \gg 1$ and are due to the transverse drift of the polarized electron when accelerated by the external electric field. The two following terms in Eq. (15) are physically similar: Namely, they arise from the slowing down of the electron during a scattering event and can be interpreted as a sudden side jump of the wave packet, as was emphasized by Berger.[19] Since the system is stationary, one expects the effect of scattering to cancel exactly the effect due to the acceleration by the electric field. This is actually verified and to this level the final transverse conductivity should vanish, a difficulty which was pointed out by Smit.[3,6]

This misleading result is obtained because the above reasoning is somewhat naive: It implies that the electron was initially at rest and that its velocity arises only from the acceleration by the external electric field. In fact, the electrons are distributed in $\vec{k}$ space and everyone of them undergoes a side jump $2\lambda\vec{S}\times\delta\vec{k}$ upon a scattering event with momentum change $\delta\vec{k}$. In the absence of external electric field, the distribution function (either Fermi or Boltzmann) has spherical symmetry around $\vec{k} = 0$, and the sum of these side jumps gives zero contribution to the electrical current. When an external electric field is applied, the spherical symmetry is broken and a twofold contribution results.

First, because of the longitudinal shift $-e\vec{E}\tau/\hbar$ of the distribution function, the sum of the side jumps of all the electrons no longer vanishes; this yields the above-mentioned contribution $-\sigma^a_{yx} - \sigma^b_{yx}$ to the transverse conductivity.

Second, because of the energy term $e\vec{E}\cdot\vec{r}$ in the Hamiltonian, a transverse shifting of the distribution function occurs, as a consequence of energy conservation upon scattering (see Fig. 2). As shown by Nozières and Lewiner, this transverse shift of the distribution function provides a further contribution $-\sigma^a_{yx} - \sigma^b_{yx}$ [the last two terms in Eq. (15)].

We have represented in Fig. 3 the time variation of the transverse position of an electron. Figure 3(a) corresponds to the incomplete result and zero transverse conductivity. Figure 3(b) corresponds to the final result; the side drift during the acceleration by the electric field is compensated by the nonzero average value of k_y due to the transverse shift of the distribution function. In this picture it might appear that only the side-jump contribution remains.[8] Actually, the six terms in Eq. (15) are identical (with various signs) and one may argue that the cancellations occur from different manners. In any case, one cannot ignore the side-drift contribution, since it becomes dominant in the limiting case $\omega\tau \gg 1$.

The final result in the case $\omega\tau \ll 1$ [Eq. (15)] is therefore the same as in the opposite limit [Eq. (13)], except for the change of sign:

$$\sigma^D_{yx} = -(ne^2\lambda/\hbar)\langle 2S_z\rangle , \qquad (16)$$

$$\mu^D_{yx} = -(e\lambda/\hbar)\langle 2S_z\rangle . \qquad (17)$$

For a given material, if the resistivity ρ is

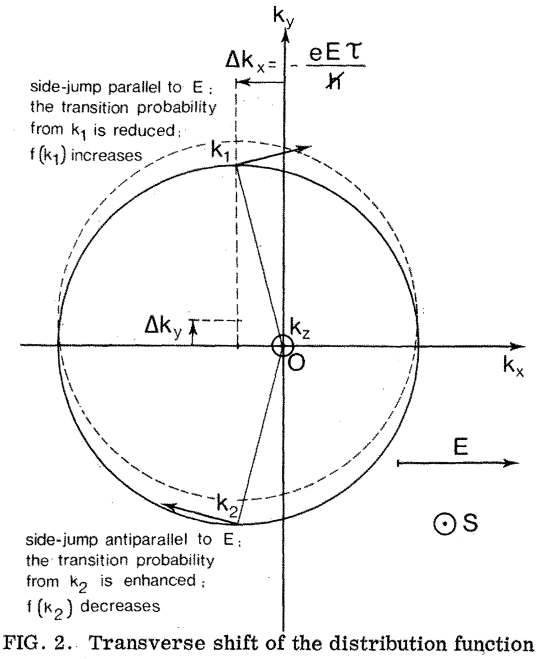

FIG. 2. Transverse shift of the distribution function and the displacement effect. The circle drawn in full line schematizes the distribution function $f(\vec{k})$, shifted from equilibrium by the trivial quantity $\Delta\vec{k}_x = -e\vec{E}\tau/\hbar$. As shown in the figure, the electron side jump upon scattering causes a change in potential energy, which results in a further shift of the distribution function $\Delta\vec{k}_y = 2\lambda e(\vec{S}\times\vec{E})m^*/\hbar$. The dashed circle schematizes the final (stationary) position of $f(\vec{k})$.

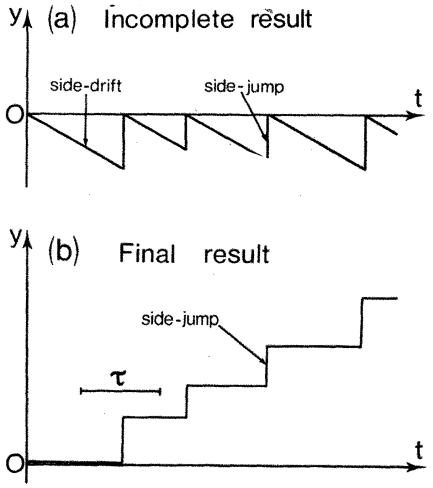

FIG. 3. Motion of an electron (schematic). The figure shows the time variation of the transverse position of the wave packet. The curve in (a) corresponds to the incomplete result (Smit, see Ref. 3); the side drift of the wave packet is compensated by the fast side jump during the scattering event. When the transverse shift of $f(\vec{k})$ is considered (see text), a further contribution results and an "average" electron behaves as shown in (b).

changed by varying the temperature or impurity content, the transverse mobility should remain constant, and if n is unchanged, the anomalous Hall constant R_{an} should be proportional to ρ^2, a behavior often observed in ferromagnetic metals.[1-3]

E. Skew-scattering contribution to the extraordinary Hall effect

A second type of contribution to the extraordinary Hall effect is due to the spin-orbit corrections to the matrix element of the scattering potential,

$$\langle\vec{k}\sigma|V|\vec{k}'\sigma\rangle = V_{\vec{k}\vec{k}'}[1 - i\lambda(\vec{k}\times\vec{k}')\cdot\vec{S}]. \qquad (18)$$

Here the scattering potential V has been assumed to be slowly varying on the scale of a unit cell and the spin-dependent terms have been limited to the lowest order ones in $\vec{k}$ and $\vec{k}'$.

Using this expression for the matrix element of V, the transition probability $W_{\vec{k}\sigma\to\vec{k}'\sigma}$, when calculated to the second Born approximation, involves spin-dependent terms of the form $(\vec{k}\times\vec{k}')\cdot\vec{S}$. The net result is a left-right asymmetry of the scattering cross section *(skew scattering)*. The corresponding contribution to the extraordinary Hall effect has been calculated by Leroux-Hugon and Ghazali,[23] taking for V a screened Coulomb potential with arbitrary screening parameter $b = 1/\nu = 4k_F^2/k_S^2$. The anomalous Hall angle θ is the relevant parameter for this effect, since it does not depend on the impurity content (which should lead, in principle, to a behavior $R_{an}\propto\rho$). The result for unit spin polarization is[23]

$$\theta_{ss}(S_z = +\tfrac{1}{2}) = \pm(2\lambda k_F/a_0^*)J, \qquad (19)$$

where the sign is plus for repulsive potentials and minus for attractive ones. The dimensionless quantity J is a function of the screening parameter $1/\nu$:

$$J = \frac{\int_0^1 F(\nu,x)dx}{\ln(1+1/\nu) - (1+\nu)^{-1}} \approx 10^{-1},$$

with

$$F(\nu,x) = -\frac{x^2(x^2+2\nu)}{(x^2+\nu)(x^2+\xi)^{1/2}}\ln\frac{(x^2+\xi)^{1/2}+x}{(x^2+\xi)^{1/2}-x} + \frac{x^3}{x^2+\nu}\ln\left(1+\frac{1}{\nu}\right)$$

and

$$\xi = 4\nu(\nu+1).$$

The anomalous Hall angle appears as the ratio of the displacement $|\vec{R}|$ at the Fermi level to some characteristic length of the range of the potential. One might wonder about the possibility for higher Born approximations to modify the above value of J. These corrections are obviously small in the

limiting case $1/\nu \gg 1$. In the opposite limit $1/\nu \ll 1$, the calculation of Lewiner *et al.*[11] shows that the lowest Born approximation gives in fact the exact result. Therefore the above expression for J gives hopefully the right order of magnitude in the whole range for $1/\nu$.

In the case of a weakly polarized electron Fermi gas ($p \ll 1$) the anomalous Hall angle becomes

$$\theta_{ss}(p) = fp\theta_{ss}(S_z = +\tfrac{1}{2}). \tag{20}$$

The factor f, of order unity, arises from the energy dependence of the transverse mobility associated with the skew-scattering effect [$f = 1 + \frac{2}{3}(E_F/\mu\theta_{ss})\partial(\mu\theta_{ss})/\partial E$]. A detailed discussion of this "statistical factor" has been given elsewhere.[24]

III. EXPERIMENTAL STUDY OF THE SPIN-DEPENDENT HALL EFFECT IN *n*-TYPE InSb

In a III-V semiconductor there is no spontaneous magnetization and a magnetic field of several kilogauss is required to obtain a complete spin polarization. But, in such a high magnetic field, the normal Hall effect is very large ($\theta_H = 1$ for $B = 10$ kG and $\mu = 10^4$ cm^2/V sec). The measurement of the anomalous Hall effect ($\theta_H \approx 10^{-3}$) is thus impossible by the classical dc method. The only way to perform this measurement is to act on the spin polarization while leaving the other parameters unchanged. The spin resonance of conduction electrons is the key to perform this experiment.

A. Choice of the material and experimental method

The choice of the material is limited to the few semiconductors where the spin resonance of conduction electrons has been observed. Moreover, in order to obtain a spin-dependent Hall effect as large as possible, the gap E_g must be small and the spin-orbit splitting Δ large. Indium antimonide seemed to us a good candidate to this experiment.

For InSb the band parameters are $E_g = 0.235$ eV and $\Delta \approx 0.9$ eV; the effective mass is $m^* = 0.0136m$ and the effective g factor $g^* = -51.4$ at the bottom of the conduction band.[25] The predicted value for the transverse mobility associated with the displacement effect is $\mu_{yx}^D = -160$ cm^2/V sec for unit spin polarization. The anomalous Hall angle associated with the skew-scattering contribution depends on the electron concentration; for a typical concentration $n \approx 10^{14}$ cm^{-3} and a mobility $\mu \approx 10^4$ to 10^5 cm^2/V sec, the corresponding effect is of the same order of magnitude as the displacement contribution. For the equilibrium polarization in a magnetic field corresponding to X-band ESR frequency ($B_0 \approx 130$ G), the resulting Hall angle $\theta_H(p)$ is of order of 10^{-4}.

The most severe limitation to the sensitivity of the method arises from the long relaxation time of the energy of the conduction electrons in InSb, giving rise to hot-electrons effects.[26] Because of these, the electric field in the sample must not exceed 0.1 V/cm, which consequently limits the allowed incident microwave power and the microwave magnetic field B_1. The discussion of the signal-to-noise ratio and of the experimental method has been given elsewhere, together with a report of preliminary experiments.[9] Before giving the results obtained with a series of variously doped InSb samples, we first recall the principle of the experimental method.

The experimental arrangement is derived from that of Juretschke (see Fig. 4).[27] The longitudinal current I_x injected into the sample is an ac current due to the microwave electric field E_x.[28] An anomalous Hall voltage in the $\vec{y}$ direction is induced by the z component of the rotating magnetization (Larmor precession around the static magnetic field $\vec{B}_0$). Since this Hall voltage involves the cross product $I_x M_z$, and both factors vary with time at the same microwave frequency $\omega/2\pi$, it contains a dc component V_{dc} that gives a measure of the effect. Our samples are sufficiently thin and resistive to leave unchanged the values of the microwave fields inside the cavity (see Appendix) and the expression for V_{dc} reduces to

$$-\frac{V_{dc}}{l} = E_y^{dc} = \tfrac{1}{2} E_x \theta_H(p)\left(\frac{2\chi' H_1 \mathrm{sgn}(g^*)}{M_0}\right), \tag{21}$$

where E_x is the amplitude of the microwave elec-

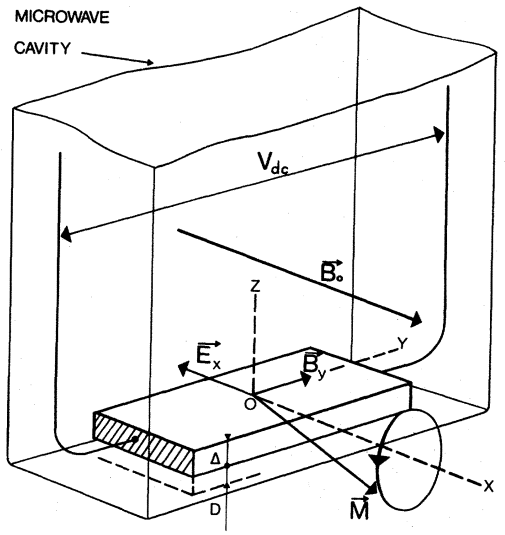

FIG. 4. Experimental arrangement. Near resonance, the magnetization $\vec{M}$ precesses around the applied field $\vec{B}_0$. The product of the microwave electric field E_x with the component M_z of $\vec{M}$ gives a dc Hall voltage along $\vec{y}$. (This figure is taken from Ref. 9.)

tric field and l is the sample length of the $\vec{y}$ direction; $\theta_H(p)$ is the anomalous Hall angle for the equilibrium polarization p in the field at which the resonance is performed, and $2\chi' H_1 \operatorname{sgn}(g^*)$ can be identified as the in-phase component of the rotating magnetization ("dispersion" curve). From the measured value of V_{dc}, Eq. (21) permits, in principle, the determination of $\theta_H(p)$.

B. Experimental procedure and results

Practical measurements of the spin-dependent Hall effect involve several difficulties. First the observed signals are rather small (typically 10^{-8} V on 10^3 -Ω source impedance) and must be optimized. This requires us to use very thin samples (50 μm) placed close to the cavity wall, in order to maximize the ratio B_1/E_x. As usual, the magnetic field is modulated (300 Hz) and a lock-in detection is used to improve the signal-to-noise ratio. In some cases, it is of appreciable help to add a dozen passages on a multichannel adder.

Second, the determination of $\theta_H(p)$ from the measurement of V_{dc} [Eq. (21)] requires a good knowledge of the microwave fields E_x and B_1. The electric field E_x is calibrated by comparing its effect on the electron temperature with the heating caused by a dc current of known value. The electron temperature is monitored by two means, since both the resistivity of the sample and the g value are temperature sensitive and can be used as thermometers. The microwave magnetic field B_1 is determined either from the measurement of the microwave power and quality factor Q of the cavity, or from the magnitude of the resonance signal observed on the resistivity of the sample (see Appendix). The simultaneous use of all these calibration methods provides an estimated accuracy of $\pm 10\%$ on the product $E_x \times B_1$.

Moreover, some difficulties are brought by the spurious effects associated with electron heating by energy absorption at resonance (bolometric effects). These effects are discussed in the Appendix; the most troublesome is the resonant Nernst effect, which yields a dispersion signal, just like the spin-dependent Hall effect. Fortunately, the magnitude of this signal can, in principle, be calculated exactly from the measured value of the dc (off-resonance) Nernst effect; this procedure is used and the calculated Nernst signal appears generally much smaller than the spin-dependent Hall signal, which warrants the validity of the measurements.

Our samples were cut from a low-doped commercial ingot ($n = N_D - N_A \approx 5 \times 10^{13}$ cm^{-3}). Various doping levels were obtained by neutron irradiation of these samples, following the procedure described by Clark and Isaacson.[29] Some samples were cut in the shape of Hall specimens and were submitted to classical measurements of the resistivity and Hall constant between 1° and 150 °K. This provides a good measure of the electron concentration and mobility. The concentration of ionized impurities, as deduced from the 40 °K mobility data, is found to be of the form $N_i \approx n + 4 \times 10^{14}$ cm^{-3}. The mobility at 1.2 °K is plotted in Fig. 5 versus electron concentration. Our results are in agreement with the data available in the literature.[30]

The other samples were polished and etched down to a thickness $\Delta \approx 50$ μm to perform the experiment of spin-dependent Hall effect. The anomalous Hall angle at the equilibrium polarization $\theta_H(p)$ is deduced according to Eq. (21); then taking for the polarization the theoretical value $p = 3\hbar\omega/4E_F$ and for the mobility μ the measured value, the transverse mobility can be scaled to unit spin polarization[31,32]:

$$\mu_{yx}^* = -\mu\theta_H(p)/p \ . \tag{22}$$

This quantity is plotted in Fig. 6 as a function of Fermi energy E_F or electron concentration n. It is negative at low electron concentrations, and displays a fast variation near $n \approx 1.5 \times 10^{14}$ cm^{-3}. For the higher concentrations, μ_{yx}^* becomes positive, but the uncertainties increase in this concentration region, because of the higher contribution of the unwanted resonant Nernst effect to the observed signal. This is the main reason for the large error bars in Fig. 6.

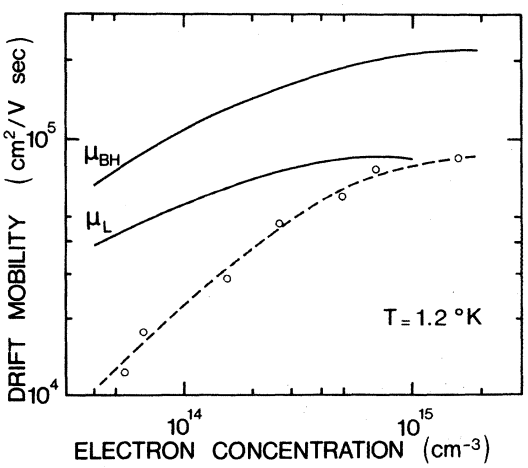

FIG. 5 Electron mobility in our InSb samples. The dashed curve has been drawn through the experimental points. The full curves are theoretical; μ_{BH} is the Brooks-Herring mobility and μ_L is obtained using Luttinger's model ($V_{\vec{k}\vec{k}'}$ = constant).

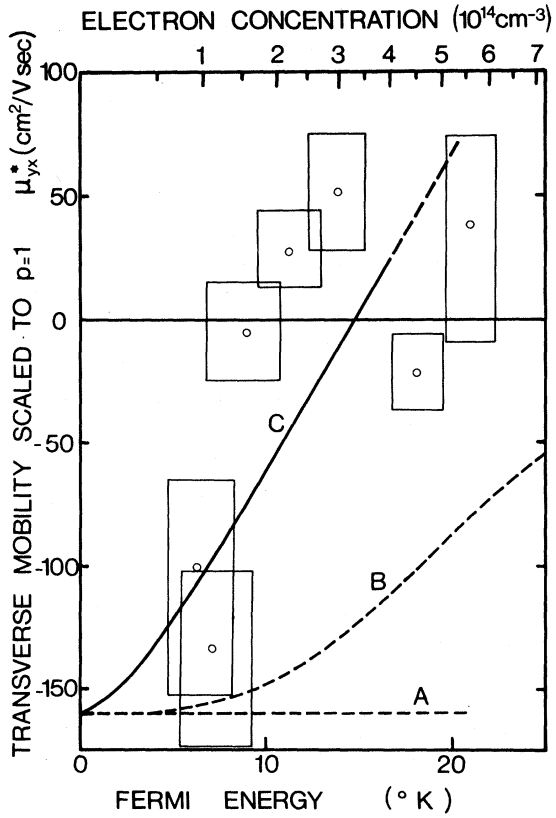

FIG. 6. Spin-dependent Hall effect in InSb: Comparison of theory with experiment. The curves are theoretical; curve A corresponds to the displacement contribution alone; curves B and C give the sum of the displacement and skew-scattering effects. The skew-scattering contribution was calculated from the theory of Leroux-Hugon and Ghazali (curve B) or from the result of Luttinger, assuming that the dominant scattering process is scattering by impurity pairs (curve C). The large uncertainties for the experimental points arise from the difficulty of measuring E_x and B_1, from the rather poor signal to noise ratio, and from the errors in substracting the unwanted resonant Nernst signal.

C. Discussion of the experimental results

The behavior of μ^*_{yx} displayed in Fig. 6 can be qualitatively understood as follows: For the less-doped samples ($n \lesssim 10^{14}$ cm^{-3}), the mobility is low because of the high compensation ratio N_A/N_D, and the displacement contribution dominates the spin-dependent Hall effect; for higher-doped samples, the skew scattering increases, canceling the displacement contribution and changing the sign of the over-all effect. The signs and order of magnitude of the predicted contributions are in concordance with this interpretation.

In order to discuss the results quantitatively, we must compare the experimental values of μ^*_{yx} with the theoretical predictions

$$\mu^*_{yx} = \mu^D_{yx} - f\mu\theta_{ss} . \tag{23}$$

The first term in Eq. (23) corresponds to the constant contribution brought by the displacement effect. The second term corresponds to the skew-scattering contribution; it involves the statistical correction factor f [$f = 1 + \frac{2}{3}(E_F/\mu\theta_{ss})\partial(\mu\theta_{ss})/\partial E$] since the experimental case corresponds to weak polarization conditions.[24]

We have calculated μ^*_{yx} from Eq. (23), taking for μ the measured mobility and for θ_{ss} the value deduced from the theory of Leroux-Hugon and Ghazali [Eq. (19)]; f has been taken from Ref. 24. Since ionized donors are attractive potentials and ionized acceptors are repulsive ones, the corresponding skew scatterings have opposite signs; this effect has been taken into account by multiplying θ_{ss} by the factor $(N_D - N_A)/(N_D + N_A) = n/N_i$; because of compensation, the impurity content N_i in our samples is greater than n ($N_i \approx n + 4\times10^{14}$ cm^{-3}), which decreases appreciably the skew-scattering contribution.

The curve resulting from our calculation is plotted in Fig. 6. In the lower concentration range, where the displacement contribution is dominant, the agreement with experiment is better than 50%, which is considered good in view of the experimental uncertainties. This agreement, with no adjustable parameter, sets up an unambiguous check of the theories of the displacement effect.

In the higher concentration range, the experimental points markedly depart from the theoretical curve. Higher Born corrections in the calculation of θ_{ss} are not likely the cause of such large discrepancies. However, these could have been expected since in the concentration region $n \lesssim 4\times10^{14}$ cm^{-3} the transport properties are not well understood and multiple scattering undoubtedly plays a dominant role. The above theory of skew scattering is therefore irrelevant to our case and we must consider the problem of skew scattering in the multiple scattering regime.

In a localized potential model ($V^{\uparrow\uparrow}_{\mathbf{k}\mathbf{k}'} = \overline{V}$ = constant), Luttinger has calculated the skew-scattering contribution arising from scattering by impurity pairs.[4] The resulting transverse mobility μ^{MS}_{yx} does not depend on the sign of the scattering potentials and can be expressed simply as a function of the displacement contribution[33] μ^D_{yx}:

$$\mu^{MS}_{yx} \approx -0.9\mu^D_{yx} = +0.9e\lambda/\hbar . \tag{24}$$

This implies that the mobility is given by the first Born approximation

$$\mu_L = \frac{\hbar e}{m^*} \frac{1}{2\pi N_i \overline{V}^2 \rho_0(E_F)} . \tag{25}$$

In fact, to be consistent, one should take into account in the mobility μ the contribution μ_{MS} from scattering by impurity pairs, which is probably dominant (i.e., $\mu_{MS} \ll \mu_L$). If Luttinger's result is corrected for this effect, Eq. (24) becomes[34]

$$\mu_{yx}^{MS} = +0.9 \frac{e\lambda}{\hbar} \left(\frac{\mu}{\mu_L} \right)^2 , \tag{26}$$

with

$$\frac{1}{\mu} = \frac{1}{\mu_L} + \frac{1}{\mu_{MS}}$$

Luttinger's model was adapted to our case by taking for $\overline{V}^2$ the average value of $V_{\vec{k}\vec{k}}^2$, on the Fermi surface, i.e.,

$$\overline{V}^2 = \left(\frac{e^2}{\epsilon\epsilon_0 2k_F^2} \right)^2 \frac{b^2}{4(1+b)} .$$

The resulting value for μ_L is plotted in Fig. 5, together with μ_{BH} obtained from Brooks-Herring formula,[35] and the experimental points. Owing to the small value of the ratio n/N_i, the corrections arising from electron-electron interactions have been neglected.[36] The large ratio μ_L/μ evidences the dominant role of multiple scattering; its order of magnitude and concentration dependence are roughly predicted by the theory of Moore[37]:

$$\frac{\mu_L}{\mu_{MS}} \propto \frac{N_i}{k_S^3} \frac{1}{k^2 a_0^{*2}} \propto n^{-7/6} .$$

This gives the energy dependence of the ratio $(\mu_{MS}/\mu_L)^2$, which permits us to predict the value of the statistical correction factor f for μ_{yx}^{MS}:

$$(\mu_{MS}/\mu_L)^2 \propto E^2 \text{ hence } f = \tfrac{7}{3} \text{ for } \mu \ll \mu_L .$$

The final contribution of multiple scattering to μ_{yx}^* is therefore

$$\mu_{yx}^{MS*} = f \mu_{yx}^{MS} \approx 2.1 \frac{e\lambda}{\hbar} \left(\frac{\mu}{\mu_L} \right)^2 . \tag{27}$$

This quantity has been computed taking for μ the measured mobility. The corresponding curve is drawn in Fig. 6. The agreement with experiment is good in view of the roughness of the model. For higher concentrations ($n \gtrsim 4 \times 10^{14}$ cm^{-3}), the model ($V_{\vec{k}\vec{k}'} = \overline{V}$) becomes very bad and our calculation overestimates the skew-scattering effect; moreover, the multiple scattering contribution to the transport properties decreases. This explains the fact that the experimental points approach the curve obtained from the theory of Leroux-Hugon and Ghazali.

IV. STUDY OF THE SPIN-DEPENDENT HALL EFFECT IN HIGHLY DOPED n-TYPE GERMANIUM

Because of its rather low spin-orbit coupling, germanium might seem at first sight unsuited for the search of the spin-dependent Hall effect, and actually the predicted effect for unit spin polarization is much smaller than in InSb. However, a great improvement is obtained in highly doped n-type germanium because there are no hot-electrons effects: The power admittable in the sample is much higher than for InSb, and the spurious resonant Nernst effect is smoothed out. On the whole, the experimental conditions are rather more favorable in germanium than in indium antimonide. Unfortunately, in the case of germanium, the simple theory of the anomalous Hall effect in a direct-gap semiconductor does not apply directly. We first develop a straightforward extension of this theory, taking into account the peculiar aspects of the band structure of germanium; then we present and discuss our experimental results.

A. Band structure and wave functions of germanium

The energy minima of the conduction band of germanium are located at the boundary of the first Brillouin zone in the [111] directions (L points). In order to build the theory of the spin-dependent Hall effect in n-type germanium, we must thus look for the wave functions in the vicinity of such a point.

At the L point of the first Brillouin zone, the conduction band is s-like and the two upper valence bands are p-like.[38] Their wave functions are linear combinations of $|X\sigma\rangle$ and $|Y\sigma\rangle$ (the $\vec{Z}$ axis has been choosen along the [111] direction). The $|Z\sigma\rangle$ state is much deeper and will not be considered here. The two upper valence bands are separated by the spin-orbit splitting Δ. Their wave functions are

$$\left.\begin{aligned} &\tfrac{1}{2}\sqrt{2}(-X - iY)|+\rangle \\ &\tfrac{1}{2}\sqrt{2}(X - iY)|-\rangle \end{aligned}\right\} \quad \text{for the upper level (energy} - E_g),$$

$$\left.\begin{aligned} &\tfrac{1}{2}\sqrt{2}(X - iY)|+\rangle \\ &\tfrac{1}{2}\sqrt{2}(-X - iY)|-\rangle \end{aligned}\right\} \quad \text{for the lower level (energy} - E_g - \Delta) .$$

Here E_g is not the semiconductor gap (0.74 eV) but the gap at the L point; $E_g = 2.08$ eV and $\Delta = 0.19$ eV.[39]

Taking into account this reduced number of bands, $\vec{k}\cdot\vec{p}$ theory has been applied to the determination of the effective-mass tensor and effective Landé factor of the conduction band.[38] The accuracy of the method appears to be of the order of 10%. We have explicitly calculated the periodic parts of the Bloch functions for the conduction band, up to second order in $\vec{k}\cdot\vec{p}$ perturbation. The result may be expressed as

$$u_{\vec{k}\sigma} = a|s\sigma\rangle - \frac{i\hbar P}{2m}\left[\left(\frac{1}{E_g}+\frac{1}{E_g+\Delta}\right)\vec{k}_\perp\cdot|\vec{R}_\perp\sigma\rangle + i\left(\frac{1}{E_g}-\frac{1}{E_g+\Delta}\right)\vec{S}_Z\cdot(\vec{k}_\perp\times|\vec{R}_\perp\sigma\rangle)\right], \tag{28}$$

where $\vec{k}_\perp = (k_X, k_Y, 0)$ and $|\vec{R}_\perp\rangle = (|X\rangle, |Y\rangle, 0)$. As in the case of a III-V semiconductor, iP is the matrix element $\langle s|p_X|X\rangle$ and a is a renormalization factor.

$$a = 1 - \frac{1}{2}\frac{E}{E_g}\frac{2E_g^2+2E_g\Delta+\Delta^2}{(2E_g+\Delta)(E_g+\Delta)}.$$

The displacement $\vec{R}$ of the wave packet can be deduced from these wave functions according to the general definition [Eq. (7)] given in Sec. II:

$$\vec{R} = i\iiint_\Omega u^*_{\vec{k}\sigma}\vec{\nabla}_{\vec{k}}u_{\vec{k}\sigma}\frac{d^3r}{\Omega} = \lambda\vec{S}_Z\times\vec{k}_\perp = \lambda\vec{S}_Z\times\vec{k},$$

with

$$\lambda = \frac{\hbar^2P^2}{m^2}\left(\frac{1}{E_g^2}-\frac{1}{(E_g+\Delta)^2}\right) = \left(1-\frac{g_\parallel}{2}\right)\frac{\hbar^2}{m}\frac{2E_g+\Delta}{E_g(E_g+\Delta)}.$$

The expression of $\vec{R}$ is very similar to that given in Sec. II, but now it involves only the Z component of the spin and the corresponding g factor.

B. Theory of the spin-dependent Hall effect in germanium

From the expression of $\vec{R}$, the spin-dependent Hall effect can be derived in the way presented in Sec. II. However, one must be careful since, for a given valley, the electron properties are anisotropic. Within the framework of our approximations, only the Z component of the spin matters, and the transverse conductivity has to be observed in the XY plane, the other configurations leading to a null result. Therefore, we first calculate the spin-dependent Hall effect for a given valley in this optimum geometry, then we consider the four-valleys system as a whole to obtain the final result.

1. Spin-dependent Hall effect in the optimum geometry

The displacement contribution to the spin-dependent Hall effect in germanium is still given by the general formula, Eq. (16),

$$\mu^D_{YX} = -\frac{e\lambda}{\hbar}\left(\frac{\partial Y}{\partial k_X}-\frac{\partial X}{\partial k_Y}\right),$$

but now we must give $\vec{R}$ its new value $\lambda\vec{S}_Z\times\vec{k}$. The result is

$$\mu^D_{YX} = -2\frac{e\lambda}{\hbar}S_Z = -0.60\ \text{cm}^2/\text{V sec} \quad \text{for } S_Z = +\tfrac{1}{2}. \tag{30}$$

The calculation of the skew-scattering effect is far more difficult because integrations over constant-energy surfaces lead to nonelementary functions. We have performed these integrations numerically after using the approximations $(k_F)^2_\perp \gg (k_F)^2_\parallel$ and $k_S^2 \gg (k_F)^2_\perp$ [here $(k_F)^2_\parallel = 2m_\parallel E_F/\hbar^2$, $(k_F)^2_\perp = 2m_\perp E_F/\hbar^2$, and k_S is the inverse screening length]. These approximations were shown to be reasonable for ionized impurity scattering in the whole metallic concentration range.[40] To zero order in λ, the mobility tensor was calculated within these approximations[41]:

$$\mu_T = \mu_{XX} = \mu_{YY} = \frac{\hbar e}{m_\perp}\frac{(4\pi\epsilon\epsilon_0)^2\hbar^2}{m_\perp e^4}\frac{(k_F)^3_\parallel}{N_i}J_T,$$
$$\mu_L = \mu_{ZZ} = \frac{\hbar e}{m_\parallel}\frac{(4\pi\epsilon\epsilon_0)^2\hbar^2}{m_\perp e^4}\frac{(k_F)^3_\parallel}{N_i}J_L, \tag{31}$$

where J_T and J_L are dimensionless functions of the screening parameter $4(k_F)^2_\parallel/k_S^2$ (in our case $J_T \approx J_L \approx 10^{-2}$). To first order in λ, the matrix element of the scattering potential becomes

$$\langle\vec{k}\sigma|V|\vec{k}'\sigma\rangle = V_{\vec{k}\vec{k}'}[1 - i\lambda(\vec{k}\times\vec{k}')\cdot\vec{S}_Z] \tag{32}$$

and the transition probability can be written

$$W_{\vec{k}\sigma\to\vec{k}'\sigma} = \frac{2\pi}{\hbar}N_i\delta(E_{\vec{k}'}-E_{\vec{k}}) \times\left(V^2_{\vec{k}\vec{k}'} - \frac{\lambda}{4\pi^2}\iiint V_{\vec{k}\vec{k}'}V_{\vec{k}'\vec{k}''}V_{\vec{k}''\vec{k}}\delta(E_{\vec{k}''}-E_{\vec{k}}) \times[(\vec{k}\times\vec{k}')+(\vec{k}'\times\vec{k}'')+(\vec{k}''\times\vec{k})]\cdot\vec{S}_Z d^3k''\right). \tag{33}$$

The terms $(\vec{k}'\times\vec{k}'')$ and $(\vec{k}''\times\vec{k})$ disappear upon integration over $\vec{k}''$. The resulting skew-scattering angle for ionized donors is

$$\theta_{ss} = -2\lambda\frac{(k_F)^2_\perp}{(k_F)_\parallel}\frac{m_\perp e^2}{4\pi\epsilon\epsilon_0\hbar^2}J' \quad \text{for } S_Z = +\tfrac{1}{2}. \tag{34}$$

One should note the similarity of this formula with the corresponding Eq. (19). Here the numerical integral J' is different from J in Eq. (19); it is plotted in Fig. 7 as a function of the screening parameter $4(k_F)^2_\parallel/k_S^2$. For $N_D = 3\times10^{17}\ \text{cm}^{-3}$ and $T = 0°\text{K}$, Eq. (34) gives $\theta_{ss} = -0.26\times10^{-4}$.

In the case of Fermi statistics and weak spin polarization, the skew-scattering effect involves a correction factor $f = 1 + \frac{2}{3}(E_F/\mu\theta_{ss})[\partial(\mu\theta_{ss})/\partial E]$, the same as in Sec. II. In the region of interest

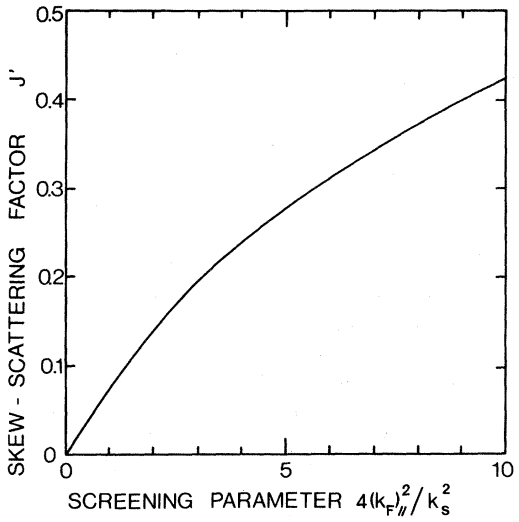

FIG. 7. Numerical integral J' for the skew-scattering effect in germanium [see Eq. (34)].

for n-type germanium, one has approximately $\mu\theta_{ss} \propto E$; hence $f \approx \frac{5}{3}$.

2. Spin-dependent Hall effect for the whole four-valleys system

Given the transverse mobility $\mu_\perp$ for $S_{Z_i} = +\frac{1}{2}$, the mobility tensor for the ith valley can be written in a simple manner, using the operators $\vec{P}_{Z_i}$ (projection along $\vec{Z}_i$) and $(\vec{S}_{Z_i}\times)$ (cross product with the Z_i component of the spin):

$$\vec{\mu}_i = \mu_T + (\mu_L - \mu_T)\vec{P}_{Z_i} + \mu_\perp(2\vec{S}_{Z_i}\times). \tag{35}$$

Because of the small value of the intervalley scattering time ($\tau_{iv} \approx 10^{-12}$ sec in As-doped Ge) an electron is scattered from one valley to another without its spin being changed ($\tau_{iv} \ll T_1$).[42,43] The mobility tensor is therefore the average value of the four tensors $\vec{\mu}_i$ ($i = 1, 2, 3, 4$). Using $\sum_i \vec{P}_{Z_i} = \frac{4}{3}$, this gives

$$\vec{\mu} = \tfrac{1}{3}(2\mu_T + \mu_L) + \tfrac{1}{3}\mu_\perp(2\vec{S}\times), \tag{36}$$

where the anisotropy has completely disappeared.

For the displacement effect, the transverse mobility thus becomes

$$\mu_{yx}^D = \tfrac{1}{3}\mu_{YX}^D = -0.20 \text{ cm}^2/\text{V sec}. \tag{37}$$

For the skew-scattering effect, the result involves the mobility anisotropy $K = \mu_T/\mu_L$.

$$\theta_{ss}^{\text{final}} = \frac{1}{3}\frac{\mu_T\theta_{ss}}{\mu} = \theta_{ss}\frac{\mu_T}{2\mu_T + \mu_L} = \theta_{ss}\frac{K}{2K+1}.$$

For $N_D = 3\times 10^{17}$ cm^{-3} and $T = 0$°K, this gives

$$\theta_{ss}^{\text{final}} = \theta_{ss}/2.2 \approx -0.12\times 10^{-4}. \tag{38}$$

C. Experimental study of the spin-dependent Hall effect in n-type germanium

In the case of germanium the principle of the experimental method is unchanged. Because of the high microwave power permissible in the sample, the signal-to-noise ratio is larger than for InSb, which permits us to perform the experiment at higher temperatures, up to $T \approx 25$°K. On the other hand, the absence of heating effects suppresses a means of calibrating the microwave electric field in the sample, which results in a higher uncertainty on the absolute value of the measured effect. For this reason the experiment was performed on a single sample, at different temperatures. The absolute uncertainty is estimated to ± 30%, but the relative uncertainty between two measurements is much better.

Arsenic was choosen as the donor impurity, because in this case the spin resonance has been extensively studied[44,45] and the resonance line is particularly narrow.[43] The donor concentration must be as small as possible to maximize the equilibrium polarization $p = 3\hbar\omega/4E_F$. However, N_D should not be below 3×10^{17} cm^{-3} since in this concentration range (intermediary zone) the resistivity becomes very high at low temperature and the one-electron model is questionable.

Our sample was cut and thinned down to 50 μm. The two adjacent slices were submitted to classical Hall and resistivity measurements at variable temperature from 1.2°K up to 300°K. The deduced electron concentration is $n \approx N_D \approx 3.1 \times 10^{17}$ cm^{-3}. The drift mobility for the two slices is plotted in Fig. 8 versus temperature. The theoretical mobility, as deduced from Eqs. (31), is 10^4 cm^2/V sec, which is 10 to 100 times larger

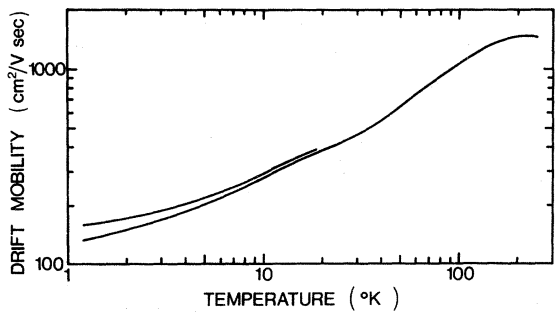

FIG. 8. Measured mobility in our germanium sample. The mobility is deduced from the resistivity measurements, assuming temperature invariance of n. The two curves in the figure correspond to the measurements performed on the two slices adjacent to our main sample. The small separation between these two curves is a check for the ingot homogeneity.

than the experimental results. This could be expected, since in our concentration range $k_S^2 \gg (k_F)_\perp^2$ and the first Born approximation fails. Moreover multiple scattering and electron correlations probably play an important role.

On the central sample, both spin-dependent Hall effect and classical ESR measurements were performed. Two experimental curves are reproduced in Fig. 9. The equilibrium polarization, as deduced from the magnitude of the ESR signal, is plotted in Fig. 10 versus temperature; above 2.5 °K it follows the theoretical law[46]

$$p = \frac{\hbar\omega}{2k_BT}\,\frac{F'_{1/2}(E_F/k_BT)}{F_{1/2}(E_F/k_BT)}\,, \tag{39}$$

where $F_{1/2}(E_F/k_BT)$ is the Fermi integral of order $\frac{1}{2}$. Below 2.5 °K the equilibrium polarization increases with decreasing temperature ($p \propto 1/T$). This type of behavior has already been observed in highly doped silicon[47,48] and arises from impurity band effects.

The anomalous Hall angle for the equilibrium polarization $\theta_H(p)$, as deduced from the magnitude of the Hall signal [Eq. (21)], is plotted in Fig. 11 versus temperature. The change of sign for $T \approx 10$ °K is quite similar to the change of sign observed in InSb at the electron concentration $n \approx 1.5\times10^{14}$ cm^{-3} and it probably bears the same interpretation.

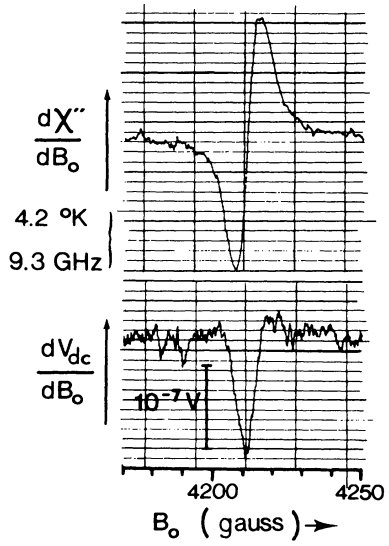

FIG. 9. Typical experimental curves for germanium. The higher curve is a conventional ESR signal (absorption derivative). The lower curve is a signal of spin-dependent Hall effect (dispersion derivative). Both signals were recorded in 50 sec.

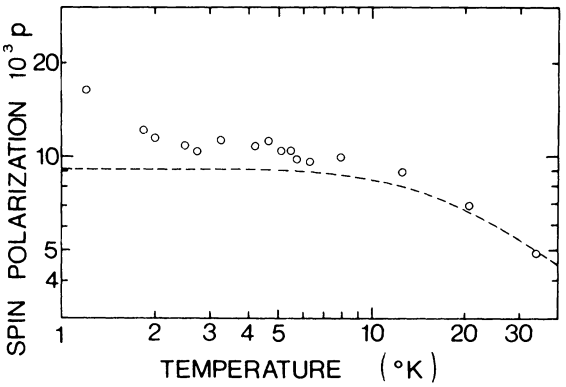

FIG. 10. Equilibrium spin polarization in the magnetic field $\vec{B}_0$. The curve is theoretical [see Eq. (39)]. The experimental points are deduced from the ESR measurements. Since no absolute measurements were performed, the vertical scale for the experimental points has been adjusted to fit the theoretical curve in the higher temperature range.

D. Discussion of the experimental results

A quantitative comparison of the experimental results with the theoretical predictions has been attempted (Fig. 12) by plotting versus temperature the quantity $\mu_{yx}^* = -\mu\theta_H(p)/p$, where μ, p, and $\theta_H(p)$ are the measured quantities. Below 2 °K, μ_{yx}^* reaches a nearly constant value -0.17 cm^2/V sec, which corresponds, within 15%, to the calculated contribution of the displacement effect ($\mu_{yx}^D = -0.20$ cm^2/V sec). This agreement, rather better than it might have been expected in view of the experimental uncertainties, constitutes a new check of the theory of the displacement effect.

At higher temperatures, μ_{yx}^* increases and changes sign. This behavior is ascribable to the growth of skew scattering, due to the increase of mobility with temperature. By comparison with the case of InSb, this interpretation is quite likely; however, a calculation of the corresponding contribution is hardly feasible, since the lower Born approximation used in Sec. IV B has been shown to be an improper approach to the transport properties of this sample, and the multiple scattering contribution is probably the dominant process. (As the observed mobility is much smaller than the calculated one, the calculated skew-scattering effect is only a few percent of the observed contribution.)

Luttinger's result on the skew-scattering effect by impurity pairs cannot be used here and the equivalent calculation in the case of germanium would be very complicated, because of anisotropy. With the lack of a quantitative theory, we may remark that the order of magnitude seems right (by analogy with InSb); moreover, the temper-

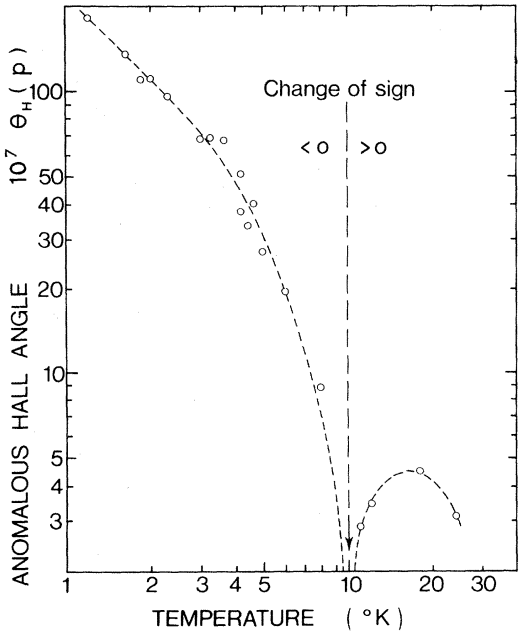

FIG. 11. Spin-dependent Hall angle for the equilibrium polarization in the magnetic field $\vec{B}_0$. The continuous curve has been drawn to guide the eye through the experimental points.

ature dependence, which occurs in the range $k_BT \lesssim E_F$, can be accounted for within a very simple model.

The energy dependence of the skew-scattering contribution in the case of InSb was given by $\mu_{yx}^{MS} \propto (\mu/\mu_L)^2$; at low energies, where multiple scattering dominates the transport properties, this gives $\mu_{yx}^{MS} \propto (\mu_{MS}/\mu_L)^2 \propto E^2$; at higher energies, $\mu \approx \mu_L$, which leaves the skew-scattering contribution nearly constant. This type of behavior can be sketched by assuming two kinds of carriers. The low-energy carriers ($E < E_c$) have a low mobility μ_0 and give zero skew-scattering contribution. The high-energy carriers ($E > E_c$) have a high mobility μ' and give a skew-scattering contribution μ'_{yx} to the transverse mobility μ^*_{yx}. Whether or not the two kinds of carriers are ascribed to different bands ("impurity band" and "conduction band") is rather a matter of vocabulary.

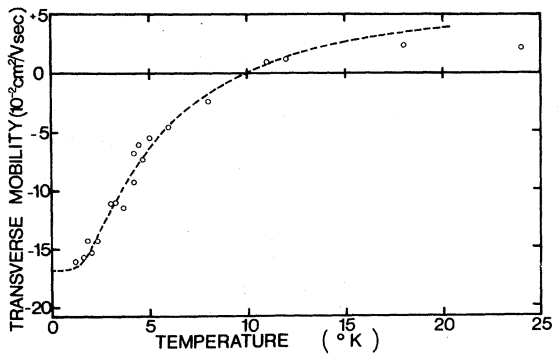

FIG. 12. Spin-dependent Hall effect in germanium: Comparison of experiment with theoretical predictions from our two carriers model. The theoretical curve corresponds to Eq. (42) (see text).

In the case of our germanium sample, we suppose $E_F < E_c$. Then at zero temperature, all the carriers are of the first kind and μ^*_{yx} corresponds to the displacement effect alone. When temperature is raised the concentration n' of carriers of the second kind increases because of thermal excitation to the energy E_c; this explains the growing up of μ^*_{yx}. In the limiting case $k_BT \ll E_F$ the concentration n' of carriers of the second kind is

$$n' = \int_{E_c}^{\infty} \rho(E) f(E)\, dE \approx \rho(E_c) \int_{E_c}^{\infty} \frac{dE}{e^{(E-E_F)/k_BT} + 1} . \tag{40}$$

The polarization p' of these carriers is given by

$$n'p' = \frac{\hbar\omega}{2} \frac{\partial n'}{\partial E_F} = \frac{\hbar\omega}{2} \frac{\rho(E_c)}{e^{(E_c-E_F)/k_BT} + 1} . \tag{41}$$

The over-all transverse conductivity is the sum of the displacement contribution and of the skew-scattering of mobile carriers. The resulting value of μ^*_{yx} is

$$\mu^*_{yx} = \mu^D_{yx} + \mu'_{yx} \frac{n'p'}{np} = \mu^D_{yx} + \mu'_{yx} \frac{\hbar\omega\rho(E_c)}{2np} \frac{1}{e^{(E_c-E_F)/k_BT} + 1} . \tag{42}$$

For an unperturbed electron density of states, the ratio $\hbar\omega\rho(E_c)/2np$ would equal 1. Although it is questionable, we assume this holds in our case. The corresponding curve for μ^*_{yx} is drawn in Fig. 12 and is seen to agree remarkably with experiment. The experimental value -0.17 cm^2/V sec has been taken for μ^D_{yx}, since anyhow it agrees with theory within 15%, and the error is most probably due to the calibration. The skew-scattering contribution μ'_{yx} and the activation energy $E_c - E_F$ have been used as adjustable parameters. The best fit is obtained with $\mu'_{yx} = -2.6\,\mu^D_{yx}$, the expected order of magnitude as compared to InSb, and $E_c - E_F \approx 6.6$°K. This value can be used to fit the longitudinal mobility to the experimental results

$$\mu = \mu_0 + (\mu' - \mu_0)\frac{n'}{n} = \mu_0 + (\mu' - \mu_0)\rho(E_c)\frac{k_BT}{n} \ln(1 + e^{-(E_c-E_F)/k_BT}) . \tag{43}$$

The corresponding curve is drawn in Fig. 13. In spite of the two further parameters μ_0 and μ', the agreement is less good than for μ_{yx}^{*}.[49,50] This could have been expected since the energy dependence of μ_{yx}^{MS} is probably steeper than that of μ [$\mu_{yx}^{MS} \propto \mu^2$ from Eq. (26)] and the model with two kinds of carriers results better for μ_{yx}^{MS} than for μ.
At any rate, the possible refinements of the present model [i.e., assume some functional dependence for $\mu(E)$ and $\mu_{yx}^{MS}(E)$] would be of little interest; any quantitative theory should take into account electron correlations, which are also the clue to the anomalous behavior of the spin polarization at low temperature.[51]

V. CONCLUSION

We have presented the theory of the spin-dependent Hall effect in semiconductors in an elementary way, stressing the physical aspects of the problem. Two contributions can be distinguished, although both of them arise from the spin-orbit interaction in the host crystal, via the admixture of p states in the conduction-band Bloch functions. The first contribution, the *displacement effect,* is due to the transverse displacement of a spin-polarized wave packet; the corresponding transverse conductivity results from the side jump undergone by such a wave packet during a scattering event. The second contribution, the *skew-scattering effect,* arises from a left-right asymmetry of the scattering cross section. The two effects are generally expected to be of the same order of magnitude, although the displacement contribution is favored in the low-mobility samples.

The existence of these two contributions has been proved by the experimental study of the spin-dependent Hall effect in n-type indium antimonide. In these experiments the spin-dependent Hall effect was separated from the much larger ordinary Hall effect by using a spin-resonance method. In the lowest-doped samples, the measured effect corresponds to the displacement contribution alone, and provides an unambiguous check of the theory. In the higher-doped samples, the skew-scattering contribution becomes important, but it is mainly ascribable to multiple scattering. A semiempirical theory of the corresponding contribution provides agreement, within a factor 2, with the experimental results.

In Sec. IV, we have extended the theory to the more complicated band structure of germanium. Thanks to intervalley scattering, the anisotropy disappears, and the theoretical results appear essentially unchanged. The experimental study has been performed in a highly doped germanium sample, as a function of temperature. At low temperature, one finds the displacement contribution alone, which gives a new check of the theory. At higher temperature, the skew-scattering contribution due to multiple scattering increases and changes the sign of the over-all effect. This contribution is hardly calculable but its temperature dependence can be simply understood in a model with two kinds of carriers.

Finally, we feel the interest of the present work is triple: First, it brings the experimental check of the theories of the displacement effect, which hopefully puts an end to a controversy initiated 20 years ago. Second, the experimental method has proved its ability for measuring very small spin-dependent Hall signals; the selectivity of spin resonance could be fully used in the study of the extraordinary Hall effect in materials with two electronic systems (i.e., resonating at two different frequencies). Last, we have shown the importance of the spin-dependent Hall effect in the study of transport properties in highly doped semiconductors and disordered media. The measurement of the multiple scattering contribution to the skew-scattering effect already provides new information. When the electron mobility becomes still smaller than in our experiments, the Hall angle associated with the displacement contribution should not increase indefinitely. Its behavior might provide a means of characterization of the conduction mechanism.

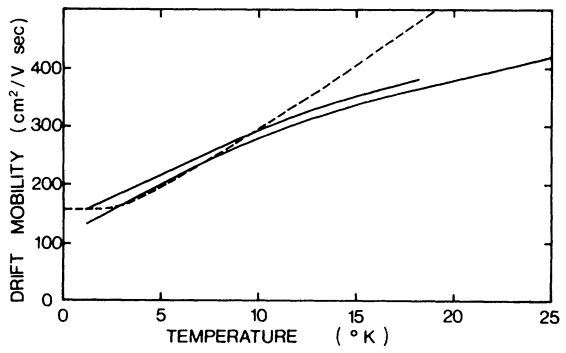

FIG. 13. Comparison of the mobility data with theoretical predictions from our two carriers model. The experimental data (full curves) correspond to the measurements performed on the two slices adjacent to our main sample. The dashed curve is theoretical; the additional parameters in Eq. (43) have been adjusted ($\mu_0 = 160$ cm^2/V sec and $\mu' \approx 1000$ cm^2/V sec).

ACKNOWLEDGMENTS

The constant help and guidance of Professor I. Solomon is gratefully acknowledged. The author is also indebted to Professor P. Nozières and

Dr. C. Lewiner for several invaluable discussions on the theory of the spin-dependent Hall effect. The preparation of the InSb samples by neutron bombardment was kindly performed by Dr. Y. Quéré and Dr. J. Mory, from Commissariat à l' Energie Atomique, and the early measurements for the characterization of these samples were done in the laboratory of Dr. H. Rodot, in Meudon-Bellevue.

APPENDIX: ELECTROMAGNETIC FIELDS INSIDE THE SAMPLE–BOLOMETRIC EFFECTS

The electromagnetic fields in the microwave cavity have been calculated by Juretschke.[27] If Δ is the sample thickness and D the distance between the sample and the bottom of the cavity, then the microwave fields inside the sample are of the form

$$H_y = h\left(\cos k_1 D \cos k_2 z - \frac{2i}{\delta^2 k_1 k_2}\sin k_1 D \sin k_2 z\right)e^{-i\omega t},$$

$$E_x = \frac{i\mu_0\omega}{k_1}h\left(\sin k_1 D \cos k_2 z - \frac{ik_1 k_2 \delta^2}{2}\cos k_1 D \sin k_2 z\right)e^{-i\omega t},$$

with $k_0 = \omega/c$ and $k_1 = k_0\sqrt{\epsilon_1}$, where ϵ_1 is the dielectric constant of medium I (see Fig. 14). The wave vector k_2 inside the sample is complex because of absorption by Joule heating and by spin resonance; $k_2 \approx (1+\chi'/2+i\chi''/2)(1+i)/\delta$, where δ is the skin depth, and χ' and χ'' are, respectively, the real and imaginary parts of the magnetic susceptibility of the sample at the frequency $\omega/2\pi$. Moreover we have supposed $\sigma \gg \epsilon\epsilon_0\omega$ and $\chi', \chi'' \ll 1$. The magnetic field h in Eqs. (44) can be expressed as a function of the magnetic field H_{inc} of the incoming wave in region III:

$$h = 2H_{\text{inc}}\left(\cos k_1 D \cos k_2 \Delta - \frac{2i}{\delta^2 k_1 k_2}\sin k_1 D \sin k_2 \Delta + i\frac{k_0}{k_1}\sin k_1 D \cos k_2 \Delta + \tfrac{1}{2}k_0 k_2 \delta^2 \cos k_1 D \sin k_2 \Delta\right)^{-1} \tag{45}$$

(a) The dc electric field generated by the spin-dependent Hall effect can be deduced from the expressions of $\vec{E}$ and $\vec{H}$.

$$E_y^{\text{dc}} = \tfrac{1}{2}\theta_H(p)\,\text{Re}\left(\frac{M_z}{M_0}E_x^*\right) = \tfrac{1}{2}\theta_H(p)\frac{\text{sgn}(g^*)}{M_0}\text{Re}[(i\chi' - \chi'')E_x^* H_y]. \tag{46}$$

In our case, $\Delta \ll \delta \ll 1/k_0, 1/k_1$; then

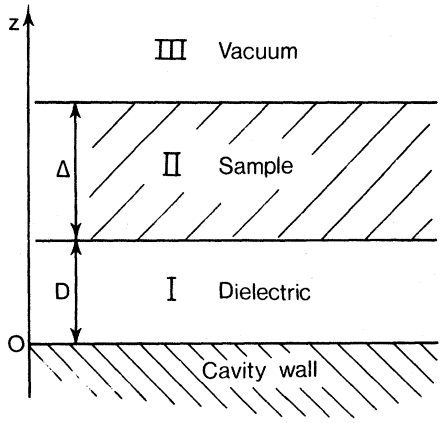

FIG. 14. Nature of the media encountered by the microwave fields from the bottom of the cavity.

$$E_y^{\text{dc}} = \theta_H(p)\,\text{sgn}(g^*)\frac{2H_{\text{inc}}^2\mu_0\omega(D+z)}{M_0[1+4(D\Delta/\delta^2)^2]}\left(\chi' + \frac{2Dz}{\delta^2}\chi''\right). \tag{47}$$

This quantity may be averaged over z inside the sample; then if one uses $D\Delta \ll \delta^2$, $H_{\text{inc}} = \frac{1}{2}h = H_1$, and $|E_x| = \mu_0\omega h(D+\Delta/2)$, this gives

$$E_y^{\text{dc}} = \tfrac{1}{2}|E_x|\,\theta_H(p)\frac{2\chi' H_1 \text{sgn}(g^*)}{M_0}. \tag{48}$$

(b) The power dissipated in the sample per unit volume is given by the first derivative of the Poynting's vector $P = \frac{1}{2}\text{Re}(E_x^* H_y)$; it gives

$$-\frac{dP}{dz} = \frac{2\mu_0\omega H_1^2}{\delta^2}[2(D+z)^2 + \delta^2\chi'' + 4z(D+z)\chi']. \tag{49}$$

The first term in the brackets corresponds to the Joule heating by the microwave electric field. The resulting contribution to $-dP/dz$ can be written $\frac{1}{2}\sigma E_x^2(z)$. The two other terms in Eq. (49) are due to the energy absorption near spin resonance. This energy, collected by the spin system, is transferred to the kinetic energy of the electrons, then to the lattice. Owing to the long relaxation time ($\tau_\epsilon \approx 10^{-7}$ sec) of the kinetic energy of the conduction electrons in InSb, the electron temperature is modified by this heating, which gives rise to many effects on the transport properties (the so-called *bolometric effects*).

A typical bolometric effect is the variation of resistivity near spin resonance; this effect arises from the temperature dependence of the mobility. It has been used as a means of detecting the resonance[52]; in our experiments, the measurement of the corresponding signal provides a calibration of the microwave magnetic field B_1.

In the method used to measure the spin-dependent Hall effect, there is no injected current in the sample, and the only bolometric effects can arise from the thermoelectric voltages, due to inhomogeneous Joule heating by the microwave electric field E_x. These thermoelectric voltages are associated with a thermoelectric field $\vec{e}$ of the form $\vec{e} = \vec{\vec{A}}\vec{\nabla}(\Delta T)$, where ΔT is the increase of electronic temperature due to the heating by E_x, and $\vec{\vec{A}}$ is a transport coefficient. When additional energy is absorbed near resonance, the resulting increase of electronic temperature δT produces a variation $\delta\vec{e}$ of the thermoelectric field:

$$\delta\vec{e} = \vec{\vec{A}}\vec{\nabla}(\delta T) + \frac{d\vec{\vec{A}}}{dT}\delta T\vec{\nabla}(\Delta T) = \delta\vec{e}_1 + \delta\vec{e}_2 .$$

The two terms in $\delta\vec{e}$ correspond to two types of effects: The first ones are proportional to the incident microwave power P, and the second ones to P^2.

In our experiments, the largest contribution to $\vec{e}$ is provided by the Nernst effect $[e_y = QB_0 d(\Delta T)/dz]$ and both types of resonant effects have been observed. The term $\delta\vec{e}_1$ is proportional to $d(\delta T)/dz$, i.e., to $4(D+2z)\chi'$ from Eq. (49). The term $\delta\vec{e}_2$ is proportional to δT, i.e., to $\delta^2\chi''$ [the term proportional to χ' in Eq. (49) is negligible in this case since $\Delta, D \ll \delta$]. The spurious signal associated with $\delta\vec{e}_2$ is not very troublesome since it has the shape of an absorption curve, whereas the Hall signal is proportional to dispersion; moreover $\delta\vec{e}_2$ is proportional to P^2, and can be eliminated by operating at low microwave power. The spurious signal associated with $\delta\vec{e}_1$ is more embarrassing, since it behaves quite similarly to the studied Hall signal. Fortunately its magnitude can be calculated from Eq. (49) and from the measured value of the dc Nernst effect $\vec{e}$: Taking the ratio of the gradients of the first and third terms in Eq. (49), we find

$$\frac{\delta e_1}{e} = \frac{D+2z}{D+z}\chi' .$$

When averaged over z, this gives a predicted value for δe_1 of

$$\delta e_1 = e\,\frac{\Delta + D}{\Delta + 2D}2\chi' .$$

In analyzing our experimental results, this predicted value of δe_1 was subtracted from the observed signal. The susceptibility χ' was given its theoretical value, a somewhat questionable point. However, the Hall signal was mostly much larger than δe_1, which justifies the use of this procedure. For higher doped samples ($n \gtrsim 4\times 10^{14}$ cm^{-3}) the two effects become of the same order of magnitude, which explains the relatively large uncertainties in Fig. 6 in this concentration region.

---

*Equipe de Recherche du Centre National de la Recherche Scientifique.

[1]For a critical review of both experiment and theory of the extraordinary Hall effect in ferromagnetics, see F. E. Maranzana, Phys. Rev. 160, 421 (1967).

[2]R. Karplus and J. M. Luttinger, Phys. Rev. 95, 1154 (1954).

[3]J. Smit, Physica (Utr.) 21, 877 (1955); 24, 39 (1958).

[4]J. M. Luttinger, Phys. Rev. 112, 739 (1958).

[5]E. N. Adams and E. I. Blount, J. Phys. Chem. Solids 10, 286 (1959).

[6]J. Smit, Phys. Rev. B 8, 2349 (1973).

[7]L. Berger, Phys. Rev. B 8, 2351 (1973).

[8]S. K. Lyo, Phys. Rev. B 8, 1185 (1973); S. K. Lyo and T. Holstein, *ibid.* 9, 2412 (1974).

[9]J.-N. Chazalviel and I. Solomon, Phys. Rev. Lett. 29, 1676 (1972).

[10]A. Bastin, C. Lewiner, and N. Fayet, J. Phys. Chem. Solids 31, 817 (1970).

[11]C. Lewiner, O. Betbeder-Matibet, and P. Nozières, J. Phys. Chem. Solids 34, 765 (1973).

[12]P. Nozières and C. Lewiner, J. Phys. (Paris) 34, 901 (1973).

[13]E. O. Kane, J. Phys. Chem. Solids 1, 249 (1957).

[14]J. C. Slater, *Quantum Theory of Molecules and Solids* (McGraw-Hill, New York, 1965), Vol. 2, App. 5, p. 455.

[15]W. Zawadzki and W. Szymańska, Phys. Status Solidi B 45, 415 (1971).

[16]E. N. Adams, J. Chem. Phys. 21, 2013 (1953).

[17]Y. Yafet, in *Solid State Physics*, edited by F. Seitz and D. Turnbull (Academic, New York, 1963), Vol. 14, pp. 1–98.

[18]A. M. de Graaf and A. W. Overhauser, Phys. Rev. 180, 701 (1969).

[19]L. Berger, Phys. Rev. B 2, 4559 (1970).

[20]R. C. Fivaz, Phys. Rev. 183, 586 (1969).

[21]The definition of $\vec{R}$ depends in fact on the choice of the basis Bloch functions and their relative phases: Namely, if a basis $b = \{u_{\vec{k}\sigma}e^{i\vec{k}\cdot\vec{r}}\}$ is replaced by another basis $b' = \{u_{\vec{k}\sigma}e^{-i\alpha(\vec{k})}e^{i\vec{k}\cdot\vec{r}}\}$, then from Eq. (7), $\vec{R}$ is replaced by $\vec{R}' = \vec{R} + \vec{\nabla}_{\vec{k}}\alpha(\vec{k})$. Therefore $\vec{R}$ is not an intrinsic (canonical) quantity. The physical parameter for the displacement is $\vec{\nabla}_{\vec{k}}\times\vec{R}$ (in the above change of basis, $\vec{\nabla}_{\vec{k}}\times\vec{R}' = \vec{\nabla}_{\vec{k}}\times\vec{R}$).

[22]The sum of the first and third term $\sigma^a_{yx} - \sigma'^a_{yx}$ in Eq. (15) corresponds to the current J_1 in the notation of Nozières and Lewiner (see Ref. 12). The second term σ^b_{yx} corresponds to J'_2 and the last one $-\sigma'^b_{yx}$ to J''_2. The fourth term $-\sigma'^b_{yx}$ corresponds to J_3 and the fifth one $-\sigma''^a_{yx}$ to J_4.

[23]P. Leroux-Hugon and A. Ghazali, J. Phys. C 5, 1072 (1972).

[24]J.-N. Chazalviel, Phys. Rev. B 10, 3018 (1974).

[25]R. A. Isaacson, Phys. Rev. 169, 312 (1968).

[26]R. J. Sladek, Phys. Rev. 120, 1589 (1960).

[27]H. J. Juretschke, J. Appl. Phys. 31, 1401 (1960); 34, 1223 (1963).

[28]In our experiments the samples are sufficiently resistive for the condition $RC\omega \gg 1$ being satisfied (R is the sample resistance and C the capacity between the sample and the bottom of the cavity). Therefore the ends of the sample in the $\vec{x}$ direction need not be electrically connected to the cavity walls to ensure the current flowing through the sample.

[29]W. G. Clark and R. A. Isaacson, J. Appl. Phys. 38, 2284 (1967).

[30]E. H. Putley, Proc. Phys. Soc. Lond. 73, 280 (1959).

[31]Taking for p the theoretical polarization is a somewhat questionable procedure since the measured magnetic susceptibility in low-doped InSb is known to depart from the theoretical value (see Ref. 32). However if these discrepancies are due to macroscopic inhomogeneities, the theoretical value of p is the most relevant to our experiment: The lower doped regions, whose contribution dominates the magnetic susceptibility, give only a small contribution to the transport properties and to the spin-dependent Hall effect. The possible errors involved in our procedure are hopefully lower than 50%.

[32]D. Kaplan and J. Konopka, in *Proceedings of the Ninth International Conference on the Physics of Semiconductors, Moscow, 1968* (Nauka, Leningrad, 1968), p. 1146.

[33]The numerical factor from Luttinger's work is $-\mu^{MS}_{yx}/\mu^{D}_{yx} = \frac{17}{30} + \frac{8}{15}\ln 2 \approx 0.94$. Our own calculations give $\frac{1}{2} + \frac{8}{15}\ln 2 \approx 0.87$. Although the origin of this discrepancy could not be found, it seems of little numerical importance.

[34]The transverse mobility is proportional to a ratio of the type W_{skew}/W^2, where W is the transition probability for slowing down the electron and W_{skew} is the transition probability in the direction $\vec{S}\times\vec{k}$. Then if W_{skew} has been correctly calculated and W underestimated, the final transverse mobility must be corrected by multiplying it by the factor $(W_{calc}/W_{real})^2 = (\mu/\mu_L)^2$.

[35]See, for example, P. P. Debye and E. M. Conwell, Phys. Rev. 93, 693 (1954).

[36]M. Luong and A. W. Shaw, Phys. Rev. B 4, 2436 (1971).

[37]E. J. Moore, Phys. Rev. 160, 618 (1967).

[38]L. M. Roth, Phys. Rev. 118, 1534 (1960).

[39]G. Dresselhaus and M. S. Dresselhaus, Phys. Rev. 160, 649 (1967).

[40]J.-N. Chazalviel, thesis (Paris, 1974) (unpublished).

[41]The calculation of μ_T within these approximations can be found in J. B. Krieger, T. Meeks, and E. Esposito, Phys. Rev. B 5, 1499 (1972).

[42]W. P. Mason and T. B. Bateman, Phys. Rev. 134, A1387 (1964).

[43]J.-N. Chazalviel, J. Phys. Chem. Solids 36, 387 (1975).

[44]E. M. Gershenzon, N. M. Pevin, and M. S. Fogelson, Phys. Status Solidi B 49, 411 (1972).

[45]M. Onda and K. Morigaki, J. Phys. Soc. Jpn. 34, 1107 (1973).

[46]A. H. Wilson, *The Theory of Metals*, 2nd ed. (Cambridge U. P., Cambridge, England, 1965), Chap. 6, p. 152.

[47]H. Ue and S. Maekawa, Phys. Rev. B 3, 4232 (1971).

[48]J. D. Quirt and J. R. Marko, Phys. Rev. B 7, 3842 (1973).

[49]In fact the mobility data might better be interpreted by assuming the discontinuity to lie at the Fermi level ($E_c - E_F = 0$). In this case, the logarithm term in Eq. (43) would equal ln2, and the calculated mobility would exhibit a linear temperature dependence, which is actually observed (see Fig. 13). In Ref. 50, some transport measurements are interpreted on a similar model with an activation energy ϵ_2; however, the value ϵ_2 found in this work may seem to be irrelevant, since it is smaller than the temperatures at which the measurements are performed. Our determination of the activation energy ($E_C - E_F$) from the spin-dependent Hall data seems much more justifiable. At any rate, the fact that the same value of the activation energy cannot account for both μ and μ^*_{yx} is an indication of the roughness of the model.

[50]C. Yamanouchi, J. Phys. Soc. Jpn. 20, 1029 (1965).

[51]W. F. Brinkman and T. M. Rice, Phys. Rev. B 2, 4302 (1970).

[52]M. Guéron and I. Solomon, Phys. Rev. Lett. 15, 667 (1965).